



RESEARCH ARTICLE

Improvement of solid oxide fuel cell performance by a core-shell structured catalyst using low concentration coal bed methane fuel

Jing Yan¹ | Wenhua Guo¹ | Huili Chen¹ | Jing Shi² | Fangqin Cheng³ |
Si-Dian Li¹ | Zongping Shao^{4,5}

¹Key Lab Mat Energy Convers & Storage, Institute of Molecular Science, Shanxi University, Taiyuan, China

²Analytical Instrumentation Center, State Key Laboratory of Coal Conversion, Institute of coal chemistry, Chinese Academy of Sciences, Taiyuan, China

³Institute of Resources and Environmental Engineering, Shanxi University, Taiyuan, China

⁴State Key Laboratory of Materials-Oriented Chemical Engineering, College of Chemical Engineering, Nanjing University of Technology, Nanjing, China

⁵Department of Chemical Engineering, Curtin University, Perth, Western Australia, Australia

Correspondence

Huili Chen, Key Lab Mat Energy Convers & Storage Shanxi Province, Institute of Molecular Science, Shanxi University, Taiyuan 030006, China.
Email: huilichen@sxu.edu.cn

Funding information

Central Government's Special Fund for Local Science and Technology Development, Grant/Award Number: YDZX20191400002916; Coal Seam Gas Joint Foundation of Shanxi, Grant/Award Number: 2015012016; National Natural Science Foundation of China, Grant/Award Number: U1610254; Shanxi "1331 Project" Engineering Research Center, Grant/Award Number: 1331ERC: PT201807; Shanxi "1331 Project" Key Innovative Research Team, Grant/Award Number: 1331KIRT; Shanxi Scholarship Council of China, Grant/Award Number: 2016-010

Summary

A core-shell structured catalyst Ni-BaO-CeO₂@SiO₂ (@NBC; 7.87% Ni content) with high catalytic activity and thermal stability is prepared and utilized for partial oxidation of methane. The catalyst is introduced into the Ni-8 mol% Y-stabilized ZrO₂ anode of a conventional solid oxide fuel cell (CC) by direct spraying (denoted as P-@NBC//CC) and indirect loading as an independent catalyst layer (denoted as Y-@NBC//CC) to improve the coking resistance and cell stability when low concentration coal bed methane is used. At 800°C, the maximum power density of P-@NBC//CC and Y-@NBC//CC increases by ~26.8% and 32.8%, respectively, over that of CC (0.63 W cm⁻²). At a discharge current of 0.16 A at 800°C, the voltage of CC drops to 0 V after 16 hours. In contrast, the voltage of P-@NBC//CC decreases from 0.8 to 0.6 V within 30 hours, and that of Y-@NBC//CC decreases from 0.8 to 0.7 V over 180 hours. The manner of loading of the catalyst layer has a significant effect on the cell stability. The indirect loading mode as an independent catalyst layer has an advantage over the direct spraying method. The postmortem microstructure of the cell reveals that direct spray loading on the anode surface allows the catalyst particles to penetrate into the anode layer and blocks the anode pores, resulting in a lower porosity and higher diffusion resistance.

KEYWORDS

catalyst layer, coking resistance, methane containing fuels, solid oxide fuel cell

1 | INTRODUCTION

Solid oxide fuel cells (SOFCs) can generate power directly from chemical energy stored in the fuel into electric energy without combustion. One drawback of the state-of-art SOFCs is coke depositing on the Ni-cermet anodes when hydrocarbons are fed, which leads to a fatal destruction of the cell.¹⁻⁴ In recent years, researchers have made several attempts to improve the coking resistance of Ni-cermet anodes,⁵⁻⁸ which are mainly focused on changing the anode composition⁹⁻¹² and fuel composition.¹³⁻¹⁷ Chang et al have reported a Ni cermet anode supported cell with an independent $\text{La}_{0.7}\text{Sr}_{0.3}\text{Co}_{0.8}\text{Fe}_{0.2}\text{O}_{3-\delta}$ (LSCF) as a protective layer, which showed excellent stability for 100 hours under wet CH_4 fuel.⁵ Silva et al have used nickel-doped ceria cermet as an active catalyst layer for direct ethanol SOFC.⁶ Chang et al have found that the redox-stable double-perovskite $\text{Sr}_2\text{MoFeO}_{6-\delta}$ reforming catalyst has a stable discharge profile over 55 hours without obvious decay.⁷ A MgO-modified Ni-based anode prepared by Hua et al presents significantly more resistance to redox cycling at 800°C than the conventional Ni-Y-stabilized ZrO_2 (YSZ) cermet anode.⁸ 2.5 wt% MgO-modified Ni-SDC anode shows a peak density of 714 mW cm^{-2} at 800°C , and has great stability for more than 330 hours of operation in humidified CH_4 fuel.⁹ In addition, the 1 wt% Sn-Ni/SDC anode studied by Yang et al displays super cell stability, where the current density decreases only to 30% after operating the cell under a constant voltage of 0.8 V in humidified CH_4 for 230 hours at 700°C .¹⁰ Coal-bed methane (CBM) is an unconventional natural gas produced during the coal-mining process, which is a greenhouse gas, possesses high calorific value, and undergoes clean combustion. Presently, the utilization efficiency of CBM, especially low concentration CBM (LC-CBM; a mixture of methane and air in which the methane content is less than 30%), is very low and this leads to large amounts of emission of greenhouse gases. As a feasible approach for utilization of LC-CBM, methane partial oxidation technology converts CH_4 and O_2 into less coking-prone CO and H_2 , which are ideal fuels for SOFCs. Nickel-based catalysts typically demonstrate high catalytic activity for partial oxidation of methane. However, these nickel-based catalysts are prone to deactivation with time at high temperatures because the metal particle undergo aggregation and are susceptible to coking, both of which decrease the number of available active sites. The application of CeO_2 can greatly improve the coking resistance of the Ni-based catalyst owing to its excellent oxygen-affording capacity.^{10-12,18} For example, a Ni-loaded (Ce, Zr) $\text{O}_{2-\delta}$ (Ni/CZ) catalyst prepared by Nguyen et al shows 87% CH_4 conversion in the dry reforming of CH_4 .¹¹ Ay and Üner have designed a Ni-Co/

CeO_2 catalyst for dry reforming of methane that exhibits 65% and 70% conversion for CH_4 and CO_2 , respectively, at 700°C after 5 hours reaction.¹² Zhu et al have manufactured a core-shell Ni/nanorod $\text{CeO}_2@\text{SiO}_2$ catalyst, which has improved catalytic activity, sintering resistance, and coking resistance during the partial oxidation of methane (POM) reaction.¹³ Addition of BaO also has a positive effect on coking resistance because of its basicity. Yang et al have prepared an anode with nanostructured barium oxide/nickel (BaO/Ni) interfaces, which displays strong water absorption and low carbon deposition.¹⁹ Rosa et al have found that Ba-doped $\text{Ni}_{0.53}\text{Cu}_{0.47}\text{O}_x/\text{CGO}$ anode has a higher maximum power density (MPD) than the anode without barium doping for the direct use of dry methane in SOFC.²⁰ Coating the Ni-based catalysts with an inert species to form a core-shell structured catalyst can effectively prevent them from accumulating.²¹⁻²⁴ Ni@Ni phyllosilicate@ SiO_2 ,²¹ and Ni-Zr $\text{O}_2@\text{SiO}_2$ ²² have also been developed, and these show good stability and carbon resistance in dry reforming. Similarly, the Ni@ SiO_2 catalyst with a core-shell structure shows that small Ni nanoparticles are effective in minimizing carbon deposition on the catalyst.²³ It has been reported that larger sized Ni particles have more carbon deposits on their surface.²⁰⁻²⁴

In this study, a catalyst precursor NiO-BaO- $\text{CeO}_2@\text{SiO}_2$ with a core-shell structure (denoted as @NOBC) has been successfully prepared by coating the NiO-BaO- CeO_2 (denoted as NOBC) precursor with tetraethyl orthosilicate (TEOS) as a silicon source under alkaline conditions. The catalyst Ni-BaO- $\text{CeO}_2@\text{SiO}_2$ (denoted as @NBC) has been obtained after treatment in a H_2 atmosphere. The catalytic performance and stability of @NBC for POM have been investigated. Using two loading modes, namely, direct spraying and indirect loading as an independent catalyst layer, @NOBC is loaded onto the Ni-YSZ anode of CC and reduced in situ, denoted as P-@NBC//CC and Y-@NBC//CC, respectively. The effect of the two loading methods on the cell performance, constant-current discharge stability, and anode carbon deposition has been studied in detail.

2 | EXPERIMENTAL SECTION

2.1 | Preparation of @NOBC

The precursor NOBC was synthesized by the combustion method that involved the following specific steps. First, $\text{Ni}(\text{NO}_3)_2 \cdot 6\text{H}_2\text{O}$, $\text{Ba}(\text{NO}_3)_2$, $\text{Ce}(\text{NO}_3)_2 \cdot 6\text{H}_2\text{O}$, 1,10-phenanthroline (Phen), and lysine (Lys) were weighed according to the 5:1:10:10:20 stoichiometric ratio. Next, Phen and $\text{Ni}(\text{NO}_3)_2 \cdot 6\text{H}_2\text{O}$ were mixed and

stirred in a certain amount of distilled water at room temperature for 4 hours. $\text{Ce}(\text{NO}_3)_2 \cdot 6\text{H}_2\text{O}$ and Lys were then dissolved and stirred in a certain amount of distilled water at 70°C for 4 hours. Finally, the above two solutions were mixed and $\text{Ba}(\text{NO}_3)_2$ together with 0.50 g of polyvinyl pyrrolidone (PVP; M^{n+} and PVP in 64:5 stoichiometric ratio) was added into the solution. The resultant solution was heated until a gel formed, which was further calcined at 300°C for 3 hours and 750°C for 2 hours.

Bian's method²⁵ was used to fabricate the silicon shell. First, 1 mmol of NOBC precursor was dissolved in a mixture of 30 mL distilled water and 90 mL anhydrous ethanol followed by the addition of 1 mmol of cetyltrimethylammonium bromide (CTAB). The final solution was treated in an ultrasonic instrument for 2 hours to obtain suspension A. Similarly, 1 mmol of TEOS was dissolved into 40 mL anhydrous ethanol to form solution B. A certain amount of ammonia was then added to suspension A until the pH of the solution was ~ 10 , followed by the dropwise addition of solution B and stirring at room temperature for 2 days. The formed suspension was centrifuged, and alternately washed three times with deionized water and anhydrous ethanol. The precipitate was dried in the oven at 80°C overnight followed by treatment at 450°C for 30 minutes and 750°C for 4 hours to obtain @NOBC. The catalyst @NBC was obtained after treatment under H_2 atmosphere for 2 hours. The synthesis process of @NOBC is shown in Figure 1.

2.2 | Preparation of the independent catalyst layer

Al_2O_3 , polyvinyl butyral (PVB), and graphite in the mass ratio of 100:15:17 were weighed and ground together. About 0.20 g of the above powder was weighed in a $\Phi 13$

steel mold and pressed under a 140 MPa pressure for 30 seconds to obtain the substrate layer. Next, a certain amount of the catalyst powder, graphite, and PVB in the mass ratio of 24:5:2 were weighed and ground using a mortar. About 0.04 g of the above powder was then evenly spread on the surface of the substrate and pressed under 220 MPa pressure for 90 seconds. The double-layered catalyst sheet was obtained after calcinations at 900°C for 4 hours.

2.3 | Cell fabrication

First, 0.43 g of the mixed anode powders (YSZ, NiO, graphite, and PVB in a weight ratio of 20:30:4:5) were weighed in a $\Phi 15$ steel mold and pressed under 100 MPa for 30 seconds. Next, 0.02 g of the YSZ electrolyte powder was weighed and spread evenly on the surface of the above anode layer, and pressed under 160 MPa pressure for 60 seconds. Then the double-layered slice was calcined for 5 hours at 1400°C . Subsequently, the $\text{Sm}_{0.2}\text{Ce}_{0.8}\text{O}_2$ (SDC) slurry was evenly sprayed onto the surface of the YSZ electrolyte layer and calcined at 1300°C for 5 hours. The cathode slurry of $\text{Ba}_{0.5}\text{Sr}_{0.5}\text{Co}_{0.8}\text{Fe}_{0.2}\text{O}_{3-\delta}$ was evenly spread onto the SDC layer surface with an effective area of 0.48 cm^2 and then calcined for 2 hours at 900°C . Lastly, silver paste as the current collector was uniformly brushed on the cathode surface and dried. Silver wires were used to conduct current.

The cell was sealed using silver paste at one end of the opening quartz tube.

2.3.1 | Cell prepared by indirect loading as an independent catalyst layer

The Al_2O_3 -based catalyst was sliced downward on one end of the quartz tube and fixed using silver paste

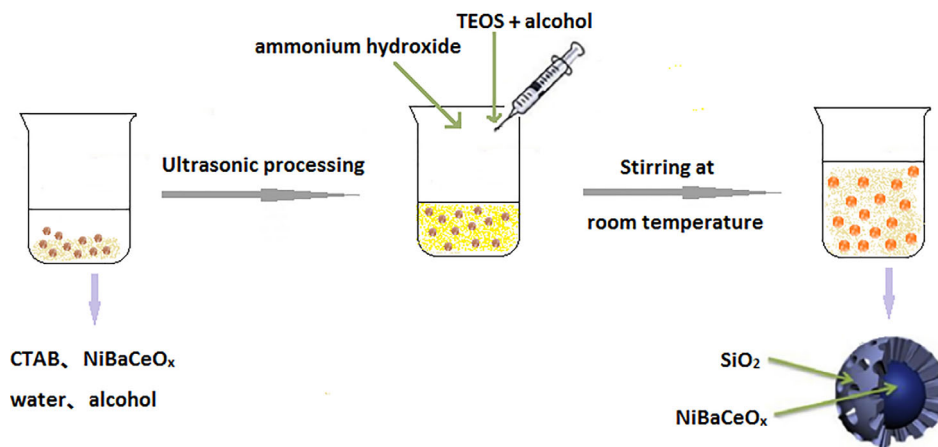


FIGURE 1 Schematic representation of synthesis of @NOBC [Colour figure can be viewed at wileyonlinelibrary.com]

(Figure 2a). The single cell anode was stuck downward with silver paste on the catalyst.

2.3.2 | Cell prepared by direct coating of the catalyst layer

About 0.8 g of catalyst powder and 0.2 g of PVB powder were mixed in a mixture of 10 mL isopropanol, 0.8 mL glycerol, and 2 mL ethylene glycol. These powders were ultrasonically dispersed for 1 hour to obtain the catalyst slurry, which was uniformly sprayed on the anode surface of cell with a thickness of $\sim 8 \mu\text{m}$ (Figure 2b).

2.4 | Characterization

X-ray diffraction (XRD) patterns were obtained using a Bruker D8 Advance powder diffractometer. The microstructure of the as-sintered catalyst was characterized by transmission electron microscopy (TEM). Scanning electron microscopy (SEM) was used for characterization of surface morphologies of samples equipped with an energy dispersive X-ray detector (EDX) for surface composition analysis. Inductively coupled plasma mass spectrometry (ICP-MS, PerkinElmer) was used to test the content of nickel. Electrochemical performance and electrochemical impedance spectroscopy (EIS) measurements of the cell were made by the IviumStat electrochemical station, Netherlands, from 600°C to 800°C with a 50°C interval. EIS was collected with the frequency ranges from 0.01 to 10^5 Hz. Before testing, the cell was reduced in situ under H_2 atmosphere (80 mL min^{-1}) for 2 hours at 700°C . When using H_2 as the fuel, the test was conducted directly. When the fuel was 30 vol% CH_4 -70 vol% air, it was purged using Ar (90 mL min^{-1}) for about 30 minutes to remove H_2 .

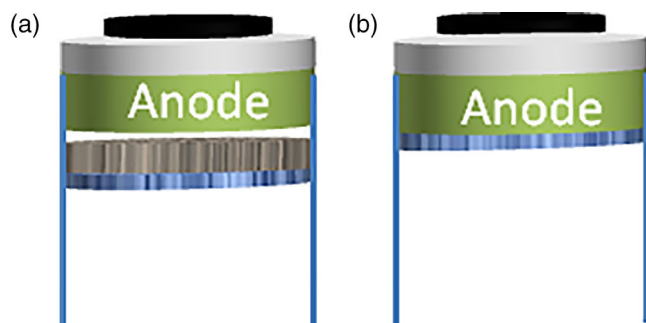


FIGURE 2 Schematic illustration of different manners of loading catalyst layer (a) indirect (b) direct [Colour figure can be viewed at wileyonlinelibrary.com]

2.5 | Catalytic performance of @NBC for POM

The catalytic performance of @NBC for POM reaction was tested in a fixed-bed reactor with the diameter of 8 mm at temperatures ranging from 500°C to 900°C . The catalyst was granulated and screened into the particle size of 40 to 60 mesh. The catalyst (0.2 g) was mixed with quartz sand (0.6 g) and placed into the middle of the reactor followed by reduced in situ for 2 hours at 800°C and subsequently cooled to room temperature under Ar. The reaction gas entered from the upper end of the reactor, flowed out from the lower end of the reactor, and passed into the gas chromatographic device to detect the contents of CH_4 , CO_2 , and CO. CO selectivity and CH_4 conversion were calculated as previously reported.²⁶

3 | RESULTS AND DISCUSSION

3.1 | Characterization of @NOBC and @NBC

ICP-MS shows that the Ni content in @NBC was 7.9 wt %. @NOBC and @NBC were characterized by XRD (Figure 3). According to Figure 3a, CeO_2 has a fluorite structure (cubic crystal) in the catalyst before reduction. Additionally, a weak NiO diffraction peak was observed, indicating that the NiO particles were sufficiently small. Using the Scherrer formula, the average particle sizes of NiO and CeO_2 were calculated as 19 nm based on the signals at 2θ of 28.21° and 42.91° , respectively. Figure 3b shows that after reduction at 800°C , the diffraction peaks that appeared at 2θ of 51.58° and 44.48° corresponded to metallic Ni, indicating exsolution of Ni particles.

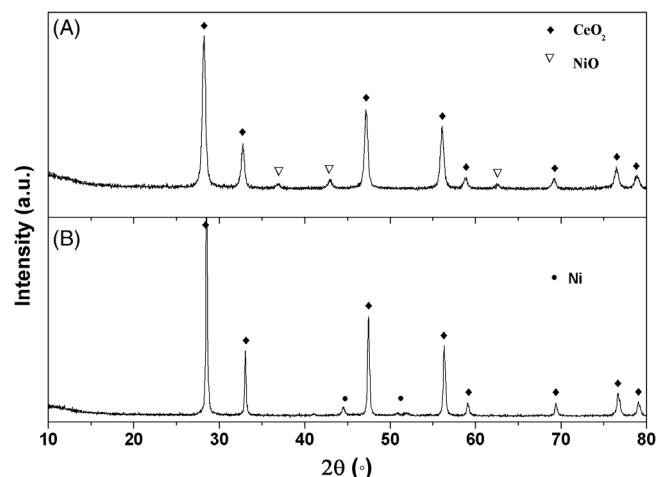
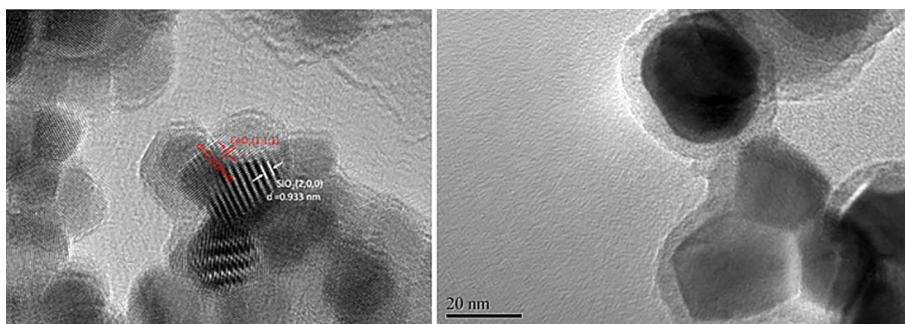


FIGURE 3 X-ray diffraction patterns of @NOBC (a) and @NBC (b)

FIGURE 4 Transmission electron microscopy image of @NOBC [Colour figure can be viewed at wileyonlinelibrary.com]



3.2 | TEM characterization of @NOBC

The morphology of @NOBC was observed by TEM. As shown in Figure 4, both CeO_2 and SiO_2 show obvious diffraction lines, such as the surface (111) of CeO_2 and the surface (200) of SiO_2 with the lattice spacing of 0.318 and 0.93 nm, respectively. As the small amount of NiO with small particle size, the diffraction line ascribed to NiO was not observed. In the synthesis process of catalyst, as the template agent CTAB was used. Porous SiO_2 shell would be formed after removing CTAB at high temperature to ensure the smooth passing of fuel gas. The smaller particle size of nickel would effectively prevent coking,²⁷ and the limit-field effect of silicon shell would effectively prevent the metal particles from moving and aggregating, so as to ensure the activity and stability of the catalyst at high temperature.

3.3 | Catalytic performance of @NBC for POM reaction

Figure 5 shows the CH_4 conversion and CO selectivity curves over the catalyst @NBC when fed with 30 vol% CH_4 -70 vol% air in the temperature of 500°C to 900°C. Below 650°C, CH_4 conversion was low and CO selectivity was zero, indicating that the main carbon product was CO_2 . When the reaction temperature was higher than 650°C, both CH_4 conversion and CO selectivity increased, and were close to 100% at 900°C and 90% at 800°C, respectively. This indicated that @NBC had a high catalytic activity for POM reaction at high temperatures. Therefore, @NBC could convert most of CH_4 and O_2 into CO and H_2 . Furthermore, it was expected that loading @NBC onto the Ni cermet anode would effectively resist coking.

Figure 6 shows the catalytic stability of @NBC when fed with 30 vol% CH_4 -70 vol% air at 750°C. The catalytic activity increased slightly from 90% up to 95% in the first 20 hours. It remained stable over the 200 hours test with both CH_4 conversion and CO selectivity of ~95%. These results indicate that @NBC had good sintering resistance

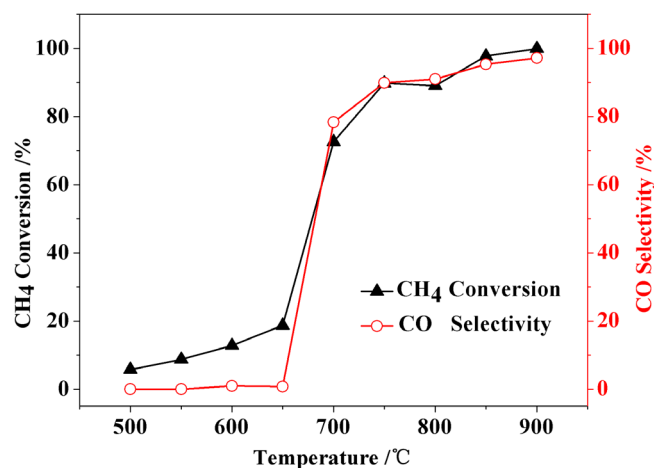


FIGURE 5 Catalytic activity of @NBC for methane oxidation reaction under 30 vol% CH_4 -70 vol% air [Colour figure can be viewed at wileyonlinelibrary.com]

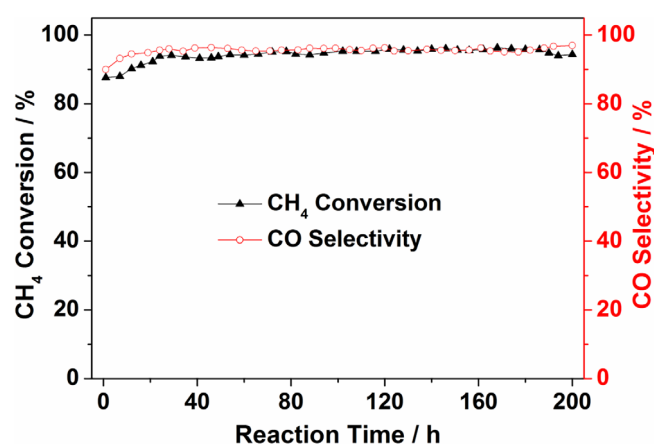


FIGURE 6 Time-dependence of the @NBC catalyst for methane oxidation reaction under 30 vol% CH_4 -70 vol% air at 750°C [Colour figure can be viewed at wileyonlinelibrary.com]

and high catalytic stability at high temperature. The catalytic performance of @NBC is compared with other classic POM catalysts and previously reported core-shell structured catalysts in Tables 1 and 2, respectively.

TABLE 1 Comparison of the catalytic performance of @NBC with other classic POM catalysts

Catalyst	Temperature (°C)	feed gas (Vol:Vol)	CH ₄ Conversion (%)	CO selectivity (%)	References
@NBC	750	CH ₄ :air = 3:7	90	90	This work
Pd/Ni/Al ₂ O ₃	800	CH ₄ :O ₂ = 2:1	31.4	61.9	28
NiFe-ZrO ₂ /Cu	800	CH ₄ :O ₂ :He = 2:1:16	60	70	29
Ni/CeO ₂ -Al ₂ O ₃	800	CH ₄ :O ₂ = 2:1	83	86	30
CeO ₂ /Fe-Cr	900	CH ₄ :O ₂ :Ar = 30:15:45	84	76	31
Co/ Mg-Al	800	CH ₄ :O ₂ = 2:1	80		32
Sr _{0.8} Ni _{0.2} ZrO ₃	800	CH ₄ :O ₂ = 2:1	75		33
LaCoO ₃ /γ-Al ₂ O ₃	800	CH ₄ :O ₂ = 4:1	36	55	34
La _{0.08} Sr _{0.92} Fe _{0.20} Ti _{0.80} O ₃	900	CH ₄ :O ₂ :Ar = 2:1:3	55		35
La _{0.3} Sr _{0.7} Fe _{0.7} Cu _{0.2} Mo _{0.1} O ₃	800	CH ₄ :O ₂ = 1.9:1	40	15	36
LaNiO ₃	800	CH ₄ :O ₂ = 2:1	85		37
0.005Rh	800	CH ₄ :O ₂ :N ₂ = 2:1:4	76.6	87.9	38
Ni/SiO ₂	750	CH ₄ :O ₂ :N ₂ = 2:1:3	70		39

Abbreviation: POM, partial oxidation of methane.

TABLE 2 Comparison of the catalytic performance of @NBC with previously reported core-shell structured catalysts

Catalyst	Reaction	Feed gas	Temperature (°C)	CH ₄ conversion (%)	Ni loading (wt%)	References
@NBC	POM	CH ₄ :air = 3:7	750	90	7.9	This work
NiO-350@meso-SiO ₂	POM	CH ₄ :O ₂ :N ₂ = 2:1:3	750	93	54.8	39
Ni@SiO ₂	DRM	CH ₄ :CO ₂ :N ₂ = 1:1:2	750	57.5	29	24
Ni@SiO ₂	DRM	CH ₄ :CO ₂ = 1:1	750	76	14.6	23
Ni-ZrO ₂ @SiO ₂	DRM	CH ₄ :CO ₂ = 1:1	750	82	6.3	22
Ni ₁₅ @HC	DRM	CH ₄ :CO ₂ = 1:1	750	45	15	24
(Ni/MgAl ₂ O ₄)@SiO ₂	DRM	CH ₄ :CO ₂ :N ₂ = 5:5:1	800	71		23
Ni-500@SiO ₂	POM	CH ₄ :O ₂ = 2:1	750	87		22
SiO ₂ @V ₂ O ₅ @Al ₂ O ₃ -(50)	Methane oxidation	CH ₄ :O ₂ = 1:1	600	22.2		43
Ni@SiO ₂	Tri-reforming of methane	CH ₄ :CO ₂ :H ₂ O:O ₂ :He = 1:0.5:3.0:0.1:0.4	750	73.1	11	44
Ni@SiO ₂	SRM	CH ₄ :H ₂ O = 1:4	700	85	20	45

Abbreviation: DRM, Dry reforming of methane; POM, partial oxidation of methane; SRM, Steam reforming of methane.

3.4 | Electrochemical performance test

The electrochemical properties of CC, P-@NBC//CC, and Y-@NBC//CC were studied when the cells were fed with 30 vol% CH₄-70 vol% air. Figure 7 shows the current-potential/power curves for the three cells at different temperatures. The catalyst-modified cells showed increased cell performance above 650°C. Table 3 lists the MPD of the cells at different temperatures. The MPDs of P-@NBC//CC increased by 26.8%, 19.6%, and 12.7% at 800°C, 750°C, and 700°C, respectively. In the case of Y-@NBC//CC, the MPDs increased by 32.9%, 27.9%, and

16.0% at the corresponding temperatures, respectively. These results indicated that the loading mode of catalyst layer had a significant effect on the cell performance at high temperatures, ie, the indirect mode was better than direct coating. At 650°C and 600°C, the two catalyst-modified cells showed similar MPDs with CC ascribed to the low catalytic activity at temperatures below 650°C, and there were large amounts of unreacted methane in the fuel. The three cells show fuel insufficiency at high current densities, which is probably related to the dilution of inert N₂ in the air. For CC, it is plausible that coking occurs and covers the active sites, further decreasing

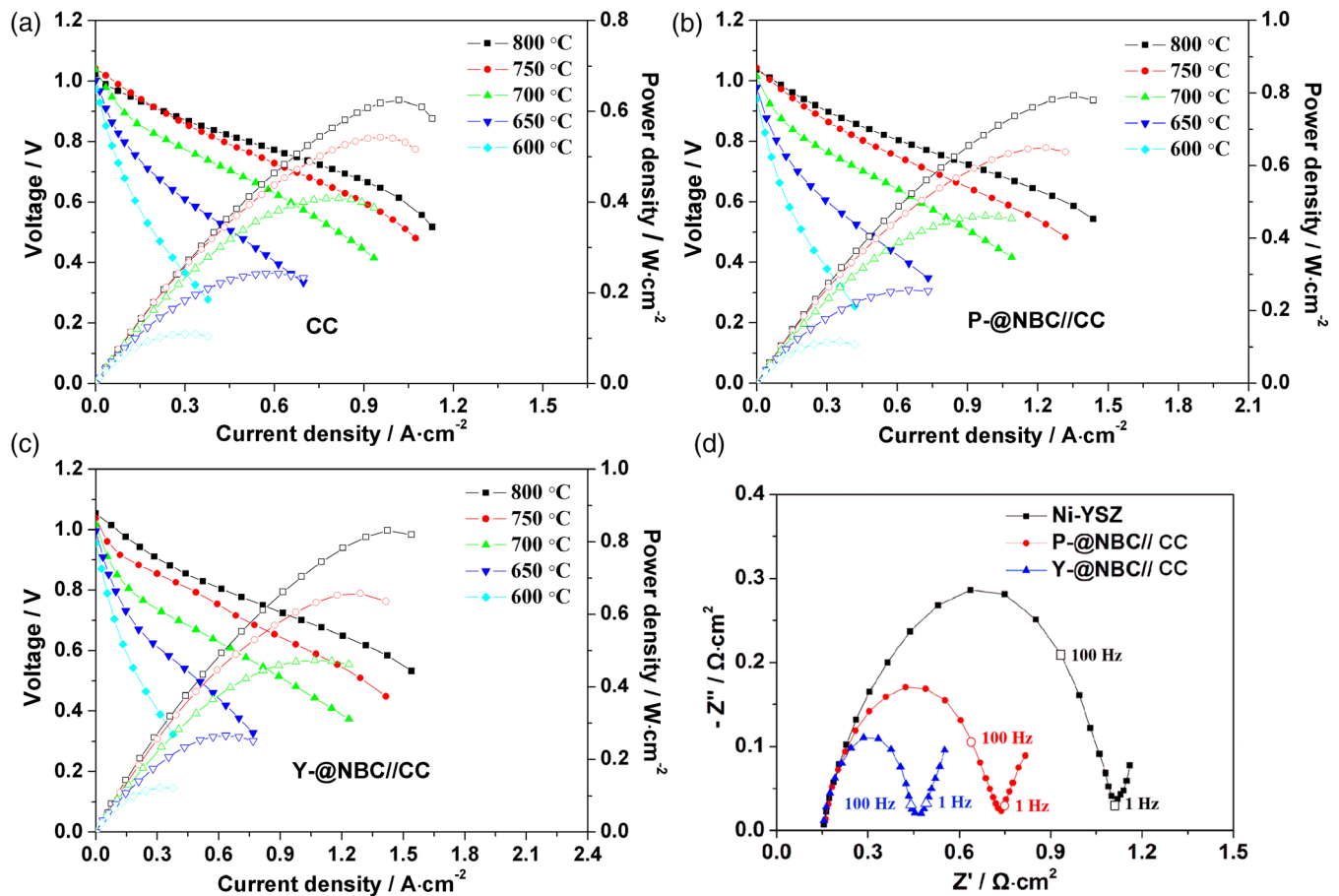


FIGURE 7 Current-potential/power curves (a) CC, (b) P-@NBC//CC, (c) Y-@NBC//CC, and the electrochemical impedance spectroscopy curves of the three cells (d) at different temperatures [Colour figure can be viewed at wileyonlinelibrary.com]

TABLE 3 Maximum power density of CC, P-@NBC//CC, and Y-@NBC//CC at different temperatures

Temperature (°C)	MPD (W cm ⁻²)		
	CC	P-@NBC//CC	Y-@NBC//CC
800	0.63	0.79	0.83
750	0.54	0.65	0.66
700	0.41	0.46	0.47
650	0.24	0.26	0.27
600	0.11	0.11	0.12

the electro-catalytic activity of the CC anode and blocking the pores in the anode. For the catalyst-modified cell with the direct coating mode, maybe the small size catalyst particles enter and block the pores in the anode layer, which is impractical for effective fuel supply.

The EIS of P-@NBC//CC, Y-@NBC//CC, and CC obtained under 30 vol% CH₄-70 vol% air flow at 800 °C also are shown in Figure 7d. It is known that the x-axis intercepts at low and high frequencies represent the total

impedance and ohmic impedance (R_o) of the SOFC, respectively. The difference between the x-axis intercepts of low and high frequencies represents the polarization impedance (R_p) of the SOFC. Figure 7d shows that the addition of the catalyst layer significantly reduced the R_p value, especially the low frequency resistances related to fuel diffusion, adsorption, and stripping. The up-folding curves at the low frequencies indicated a diffusion-controlled electrode process,⁴⁶ which agrees with the results of the I-V experiments. The R_p values for the three cells increased in the following order: CC > P-@NBC//CC > Y-@NBC//CC, further confirming the advantage of the indirect catalyst layer.

3.5 | Constant current stability of cells

Stability is another index to evaluate the applicability of the cell. Figure 8 shows the time-dependent voltages of CC, P-@NBC//CC, and Y-@NBC//CC fed with 30 vol% CH₄-70 vol% air at 0.16 A and 800 °C. Y-@NBC//CC was significantly more stable than P-@NBC//CC and CC. The

voltage of CC dropped to 0 V within 16 hours, which was related to the carbon deposition on the cell anode.⁴⁷ The voltage of P-@NBC//CC decreased from 0.8 to 0.6 V within 30 hours, while that of Y-@NBC//CC decreased from 0.8 to 0.7 V after 180 hours. The results indicate that @NBC-modified cells had better stability compared to the conventional cell, which benefits from the conversion of methane by the catalyst. In addition, the cell using the

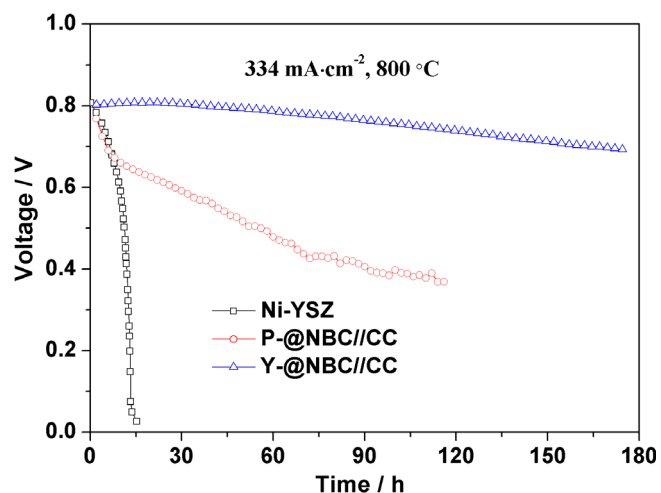


FIGURE 8 Time-dependent voltages of CC, P-@NBC//CC, and Y-@NBC//CC fed with 30 vol% CH₄-70 vol% air at 0.16 A and 800°C [Colour figure can be viewed at wileyonlinelibrary.com]

indirect catalyst layer exhibited better performance than that using the direct-coating catalyst layer.

3.6 | Cell surface analysis

It has been shown that the different loading modes have considerable effect on the electrochemical performance. The cell Y-@NBC//CC, prepared using an indirect loading mode, exhibited better performance than P-@NBC//CC, which was prepared by direct coating. Postmortem cross-sectional microstructures of the anode layer for P-@NBC//CC were characterized using SEM (Figure 9). The catalyst layer was closely bound to the anode layer without falling off, indicating that the catalyst was well-supported by spraying. At the two-phase interface between the catalyst and anode layer, the catalyst particles entered into the anode pores and blocked the anode channel, which was detrimental to efficient fuel gas diffusion and decreased the anode activity. These results are in agreement with the observed electrochemical performance.

The microstructure of the surface of the Y-@NBC//CC catalyst before (Figure 10a) and after (Figure 10b) applying constant current stability was studied. Both surfaces showed a granular porous structure, which ensured the smooth passing of fuel gas. EDX tests indicated that the carbon contents were 7.74 at% and 8.20 at% for a

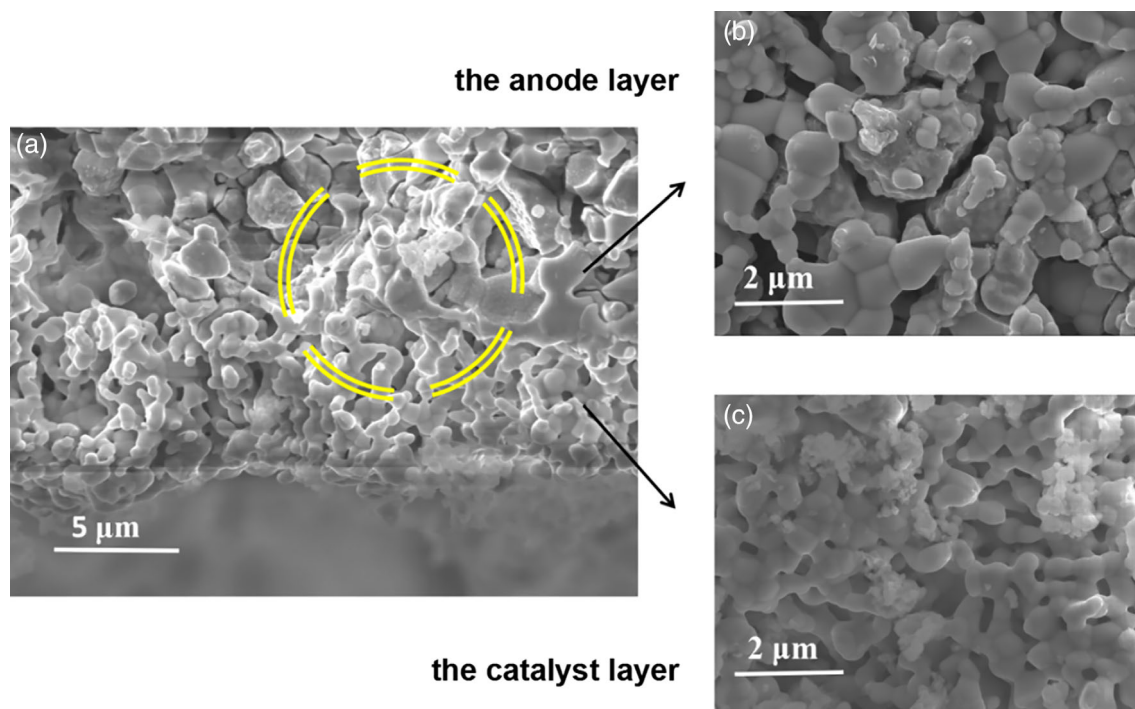


FIGURE 9 Cross-sectional scanning electron microscopy image of P-@NBC//CC at the two-phase interface between the catalyst and anode layer [Colour figure can be viewed at wileyonlinelibrary.com]

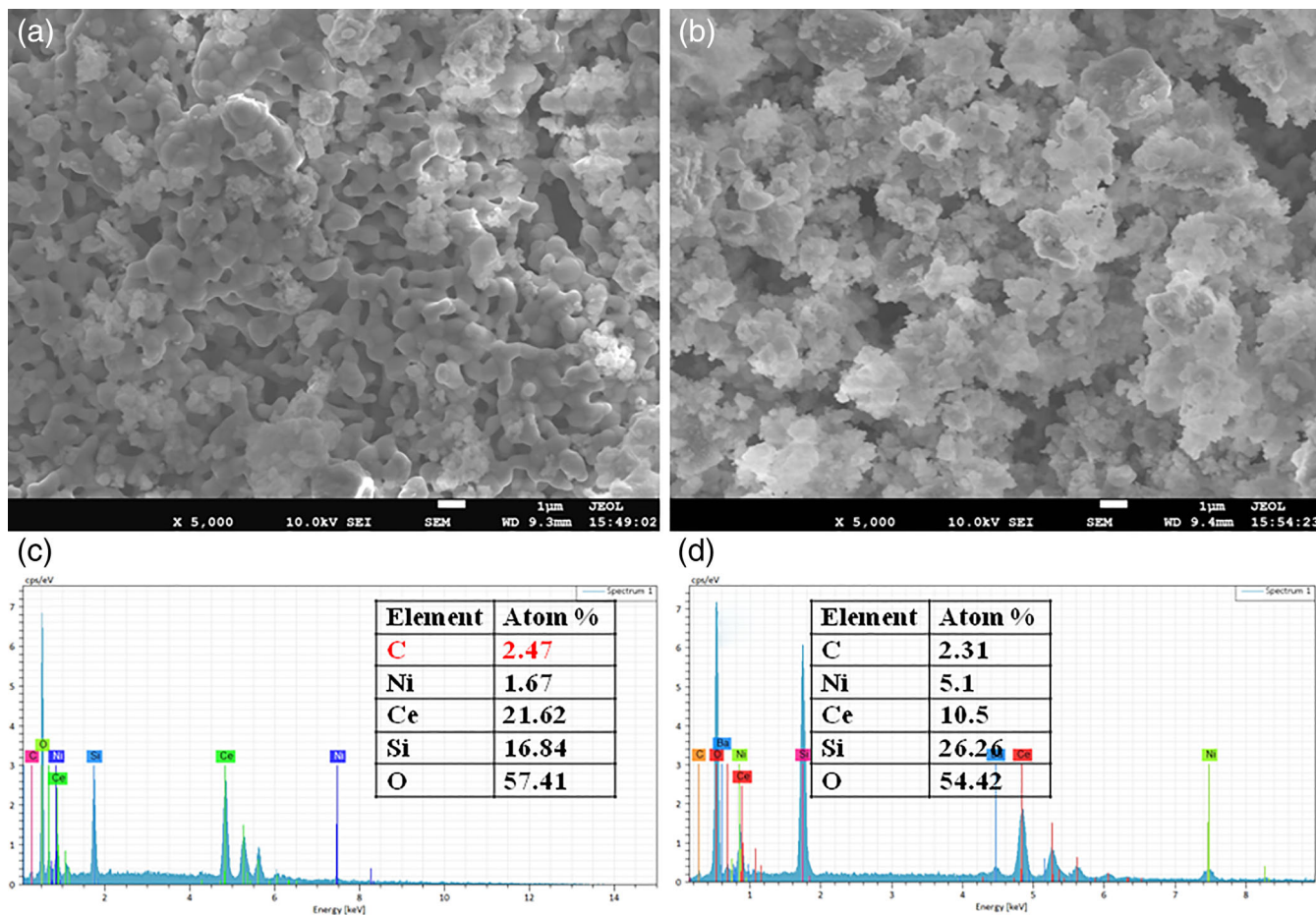


FIGURE 10 Scanning electron microscopy (SEM) and EDS spectra of the catalyst surface: SEM (a) and EDS (c) of the fresh catalyst surface, SEM (b) and EDS (d) of the catalyst surface after constant discharge for 180 hours [Colour figure can be viewed at wileyonlinelibrary.com]

fresh catalyst surface (Figure 10c,d) and an aged surface, respectively. The subtle differences indicate that the addition of the @NBC layer significantly improved the coking resistance.

4 | CONCLUSION

In this study, a core-shell catalyst @NBC with small particle size was prepared to improve the thermal stability of the catalyst NBC. The electrochemical performance and stability of an SOFC was improved by introducing @NBC into the Ni-YSZ anode. At 800°C, the MPD of P-@NBC//CC and Y-@NBC//CC increased by ~26.8% and 32.8%, respectively, over that of CC (0.63 W cm⁻²). At a discharge current of 0.16 A at 800°C, the voltage of CC dropped to 0 V after 16 hours. In contrast, the voltage of P-@NBC//CC decreased from 0.8 to 0.6 V within 30 hours, and that of Y-@NBC//CC decreases from 0.8 to 0.7 V over 180 hours. These results indicate that the

loading modes of the catalyst layer had a considerable effect on the cell performance. Direct coating the catalyst onto the anode layer deactivated the anode and was unstable because the small catalyst particles permeated the anode layer and blocked the anode pores. The indirect loading mode as an independent layer was beneficial for improving the coking resistance. The manner of loading of the catalyst layer has a significant effect on the cell stability. The indirect loading mode as an independent catalyst layer shows an advantage over the direct spraying method. The postmortem microstructure of the cell reveals that direct spray loading on the anode surface allows the catalyst particles to penetrate into the anode layer and blocks the anode pores, resulting in a lower porosity and higher diffusion resistance.

ACKNOWLEDGEMENTS

This work was supported by the Central Government's Special Fund for Local Science and Technology Development (YDZX20191400002916); National Natural Science

Foundation of China-Shanxi Coal-based Low Carbon Joint Fund (U1610254); Coal Seam Gas Joint Foundation of Shanxi (2015012016); Shanxi Scholarship Council of China (2016-010) and Shanxi '1331 Project' Key Innovative Research Team (1331KIRT), and Engineering Research Center (1331ERC: PT201807).

REFERENCES

1. Steele BCH. Material science and engineering: the enabling technology for the commercialisation of fuel cell systems. *J Mater Sci.* 2001;36(5):1053-1068.
2. Mark Ormerod R. Solid oxide fuel cells. *Chem Soc Rev.* 2003;32(1):17-28.
3. Wachsmann ED, Lee KT. Lowering the temperature of solid oxide fuel cells. *Science.* 2011;334(6058):935-939.
4. Singh B, Ghosh S, Aich S, Roy B. Low temperature solid oxide electrolytes (LT-SOE): a review. *J Power Sources.* 2017;339:103-135.
5. Chang H, Chen H, Yang G, et al. Enhanced coking resistance of a Ni cermet anode by a chromates protective layer. *J. Energ. Chem.* 2019;37:117-125.
6. da Silva AAA, Tabuti FN, Mattos LV, Steil MC, Noronha FB, Fonseca FC. Anodic layers based on doped-ceria/Ni cermet for direct ethanol fuel cells. *ECS Transactions.* 2017;78(1):1437-1445.
7. Chang H, Chen H, Yang G, et al. Enhanced coking resistance of Ni cermet anodes for solid oxide fuel cells based on methane on cell reforming by a redox-stable double perovskite $\text{Sr}_2\text{MoFeO}_{6-\delta}$. *Int J Energy Res.* 2019;43(7):2527-2537.
8. Hua B, Zhang W, Li M, et al. Improved microstructure and performance of Ni-based anode for intermediate temperature solid oxide fuel cells. *J Power Sources.* 2014;247:170-177.
9. Yang Q, Chai F, Ma C, Sun C, Shi S, Chen L. Enhanced coking tolerance of a MgO-modified Ni cermet anode for hydrocarbon fueled solid oxide fuel cells. *J Mater Chem A.* 2016;4:18031-18036.
10. Yang Q, Chen J, Sun C, Chen L. Direct operation of methane fueled solid oxide fuel cells with Ni cermet anode via Sn modification. *Int J Hydrogen Energy.* 2016;41(26):11391-11398.
11. Nguyen TGH, Tran DL, Sakamoto M, et al. Ni-loaded (Ce,Zr) $\text{O}_{2-\delta}$ -dispersed paper-structured catalyst for dry reforming of methane. *Int J Hydrogen Energy.* 2018;43(10):4951-4960.
12. Ay H, Üner D. Dry reforming of methane over CeO_2 supported Ni, Co and Ni-Co catalysts. *Appl. Catal. B-Environ.* 2015;179:128-138.
13. Zhu S, Lian X, Fan T, et al. Thermally stable core-shell Ni/nanorod $\text{CeO}_2/\text{SiO}_2$ catalyst for partial oxidation of methane at high temperatures. *Nanoscale.* 2018;10(29):14031-14038.
14. Muraza O, Galadima A. A review on coke management during dry reforming of methane. *Int J Energy Res.* 2015;39(9):1196-1216.
15. Li S, Gong J. Strategies for improving the performance and stability of Ni-based catalysts for reforming reactions. *Chem Soc Rev.* 2014;43(21):7245-7256.
16. Pakhare D, Spivey J. A review of dry CO_2 reforming of methane over noble metal catalysts. *Chem Soc Rev.* 2014;43(22):7813-7837.
17. Liu C, Ye J, Jiang J, Pan Y. Progresses in the preparation of coke resistant Ni-based catalyst for steam and CO_2 reforming of methane. *ChemCatChem.* 2011;3(3):529-541.
18. Das S, Ashok J, Bian Z, et al. Silica-ceria sandwiched Ni core-shell catalyst for low temperature dry reforming of biogas: coke resistance and mechanistic insights. *Appl. Catal. B-Environ.* 2018;230:220-236.
19. Yang L, Choi Y, Qin W, et al. Promotion of water-mediated carbon removal by nanostructured barium oxide/nickel interfaces in solid oxide fuel cells. *Nat Commun.* 2011;2:1-9.
20. La Rosa D, Sin A, Faro ML, Monforte G, Antonucci V, Aricò AS. Mitigation of carbon deposits formation in intermediate temperature solid oxide fuel cells fed with dry methane by anode doping with barium. *J Power Sources.* 2009;193:160-164.
21. Li Z, Jiang B, Wang Z, Kawi S. High carbon resistant Ni@Ni phyllosilicate@ SiO_2 core shell hollow sphere catalysts for low temperature CH_4 dry reforming. *J. CO2 Util.* 2018;27:238-246.
22. Liu W, Li L, Zhang X, Wang Z, Wang X, Peng H. Design of Ni-ZrO₂@ SiO_2 catalyst with ultra-high sintering and coking resistance for dry reforming of methane to prepare syngas. *J CO2 Util.* 2018;27:297-307.
23. Wang F, Xu L, Shi W. Syngas production from CO_2 reforming with methane over core-shell Ni@ SiO_2 catalysts. *J. CO2 Util.* 2016;16:318-327.
24. Zhang J, Li F. Coke-resistant Ni@ SiO_2 catalyst for dry reforming of methane. *Appl. Catal. B-Environ.* 2015;176-177:513-521.
25. Bian Z, Suryawinata IY, Kawi S. Highly carbon resistant multicore-shell catalyst derived from Ni-mg phyllosilicate nanotubes@silica for dry reforming of methane. *Appl Catal B-Environ.* 2016;195:1-8.
26. Yang G, Su C, Chen Y, Tade M, Shao Z. Nano $\text{La}_{0.6}\text{Ca}_{0.4}\text{Fe}_{0.8}\text{Ni}_{0.2}\text{O}_{3-\delta}$ decorated porous doped ceria as a novel cobalt-free electrode for "symmetrical" solid oxide fuel cells. *J. Mater Chem A.* 2014;2(45):19526-19535.
27. Yen H, Seo Y, Kaliaguine S, Kleitz F. Tailored mesostructured copper/ceria catalysts with enhanced performance for preferential oxidation of CO at low temperature. *Angew. Chem.-Int. Ed.* 2012;51(48):12032-12035.
28. Enger BC, Lødeng R, Holmen A. Effects of Noble metal promoters on in situ reduced low loading Ni catalysts for methane activation. *Catal Lett.* 2010;134(1-2):13-23.
29. Wang W, Zhu H, Yang G, et al. A NiFeCu alloy anode catalyst for direct-methane solid oxide fuel cells. *J Power Sources.* 2014;258:134-141.
30. Yu C, Hu J, Zhou W, Fan Q. Novel Ni/ CeO_2 - Al_2O_3 composite catalysts synthesized by one-step citric acid complex and their performance in catalytic partial oxidation of methane. *J. Energ. Chem.* 2014;23:235-243.
31. Ma Z, Perreault P, Pelegrin DC, Boffito DC, Patience GS. Thermodynamically unconstrained forced concentration cycling of methane catalytic partial oxidation over CeO_2 FeCralloy catalysts. *Chem Eng J.* 2020;380:122470.
32. Moral A, Reyero I, Llorca J, Bimbela F, Gandía LM. Partial oxidation of methane to syngas using Co/Mg and Co/Mg-Al oxide supported catalysts. *CatalToday.* 2019;333:259-267.
33. Staniforth J, Evans SE, Good OJ, Darton RJ, Ormerod RM. A novel perovskite based catalyst with high selectivity and activity for partial oxidation of methane for fuel cell applications. *Dalton Trans.* 2014;43(40):15022-15027.
34. Brackmann R, Perez CA, Schmal M. LaCoO_3 perovskite on ceramic monoliths—pre and post reaction analyzes of the

- partial oxidation of methane. *Int J Hydrogen Energy*. 2014;39(26):13991-14007.
35. Morales M, Espiell F, Segarra M. Performance and stability of $\text{La}_{0.5}\text{Sr}_{0.5}\text{CoO}_{3-\delta}$ perovskite as catalyst precursor for syngas production by partial oxidation of methane. *Int J Hydrogen Energy*. 2014;39(12):6454-6461.
36. Meng B, Zhang H, Qin J, Tan X, Ran R, Liu S. The catalytic effects of $\text{La}_{0.3}\text{Sr}_{0.7}\text{Fe}_{0.7}\text{Cu}_{0.2}\text{Mo}_{0.1}\text{O}_3$ perovskite and its hollow fibre membrane for air separation and methane conversion reactions. *Sep. Purif Dent Tech*. 2015;147:406-413.
37. Pereniguez R, González-DelaCruz VM, Holgado JP, Caballero A. Synthesis and characterization of a LaNiO_3 perovskite as precursor for methane reforming reactions catalysts. *Appl. Catal. B-Environ*. 2010;93(3-4):346-353.
38. Berger-Karin C, Radnik J, Kondratenko EV. Mechanistic origins of the promoting effect of tiny amounts of Rh on the performance of $\text{NiO}_x/\text{Al}_2\text{O}_3$ in partial oxidation of methane. *J Catal*. 2011;280(1):116-124.
39. Li L, He S, Song Y, Zhao J, Ji W, Au CT. Fine-tunable $\text{Ni}@$ porous silica core-shell nanocatalysts: synthesis, characterization, and catalytic properties in partial oxidation of methane to syngas. *J Catal*. 2012;288:54-64.
40. Han J, Liang Y, Qin L, Zhao B, Wang H, Wang Y. $\text{Ni}@$ HC Core-Shell structured catalysts for dry reforming of methane and carbon dioxide. *Catal Lett*. 2019;149(11):3224-3237.
41. Wang Y, Fang Q, Shen W, Zhu Z, Fang Y. $(\text{Ni}/\text{MgAl}_2\text{O}_4)\text{@SiO}_2$ core-shell catalyst with high coke-resistance for the dry reforming of methane. *React Kinet Mech Cat*. 2018;125(1):127-139.
42. Ding C, Gao X, Han Y, et al. Effects of surface states over core-shell $\text{Ni}@$ SiO_2 catalysts on catalytic partial oxidation of methane to synthesis gas. *J Energ Chem*. 2015;24(1):45-53.
43. Yang E, Lee JG, Kim DH, et al. $\text{SiO}_2\text{@V}_2\text{O}_5\text{@Al}_2\text{O}_3$ core-shell catalysts with high activity and stability for methane oxidation to formaldehyde. *J Catal*. 2018;368:134-144.
44. Majewski AJ, Wood J. Tri-reforming of methane over $\text{Ni}@$ SiO_2 catalyst. *Int J Hydrogen Energy*. 2014;39(24):12578-12585.
45. Park JC, Bang JU, Lee J, Ko CH. $\text{Ni}@$ SiO_2 yolk-shell nanoreactor catalysts: high temperature stability and recyclability. *J Mater Chem*. 2010;20(7):1239-1246.
46. Chen H, Guo W, Wu Y, et al. A strategy to reduce the impact of tar on a Ni-YSZ anode of solid oxide fuel cells. *Int J Energy Res*. 2019;43(23):3038-3048.
47. Qu J, Wang W, Chen Y, Wang F, Ran R, Shao Z. Ethylene glycol as a new sustainable fuel for solid oxide fuel cells with conventional nickel-based anodes. *Appl Energy*. 2015;148:1-9.

How to cite this article: Yan J, Guo W, Chen H, et al. Improvement of solid oxide fuel cell performance by a core-shell structured catalyst using low concentration coal bed methane fuel. *Int J Energy Res*. 2020;1-11. <https://doi.org/10.1002/er.5301>